Journal of Sol-Gel Science and Technology (2019) 91:514–522
https://doi.org/10.1007/s10971-019-05057-5

ORIGINAL PAPER: NANO- AND MACRO-POROUS MATERIALS (AEROGELS, XEROGELS, CRYOGELS, ETC.)

Check for updates

# Mechanical strengths and thermal properties of titania-doped alumina aerogels and the application as high-temperature thermal insulator

Min Gao[1,2] · Benxue Liu[1] · Ping Zhao[2] · Xibin Yi[1] · Xiaodong Shen[1] · Yue Xu[1,2]

Received: 24 December 2018 / Accepted: 15 June 2019 / Published online: 26 June 2019


## Abstract

Alumina ($Al_2O_3$)-based diphasic aerogels have better physical properties than those of pure $Al_2O_3$ aerogel according to previous studies. In the present research, we focused on an alumina–titania ($Al_2O_3$-$TiO_2$) diphasic aerogel. A series of $Al_2O_3$ aerogels were synthesized and studied with and without minor $TiO_2$ dopants (up to 10 mol%). We found that the pure $Al_2O_3$ aerogel, which had the fiber-like particles, was stronger than those with $TiO_2$ dopants that possessed the sphere-like particles. However, the sphere-like particles make the $TiO_2$-doped $Al_2O_3$ aerogel (with 3 mol% $TiO_2$) possessing the largest specific surface area (SSA) of 650 $m^2$/g, much larger than that of the pure $Al_2O_3$ aerogel (326 $m^2$/g). This work proved that fiber-like particles enhance strength but reduce SSA of $Al_2O_3$ aerogel. At last, ceramic fibers reinforced $Al_2O_3$ aerogel composites with the sizes of 20 cm width × 20 cm length × 1 cm thickness were fabricated. The aerogel composites possessed a thermal conductivity of 0.136 W/m K at 1000 °C, better than those of the ceramic fiber blankets itself (0.30 W/m K), indicating potential application as high-temperature thermal insulator.

## Graphical Abstract

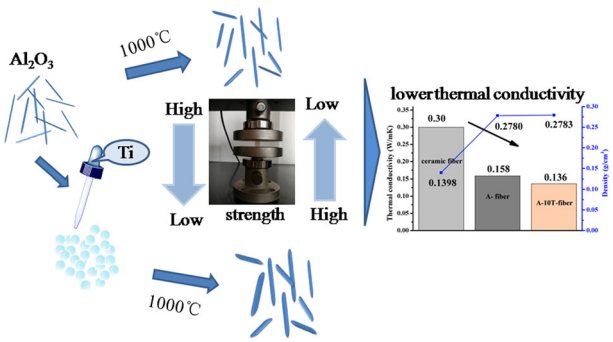


**Supplementary information** The online version of this article (https://doi.org/10.1007/s10971-019-05057-5) contains supplementary material, which is available to authorized users.

✉ Benxue Liu
liubenxue@gmail.com

✉ Xibin Yi
yixb@sdas.org

[1] Qilu University of Technology (Shandong Academy of Sciences), Advanced Materials Institute, Shandong Provincial Key Laboratory for Special Silicone-Containing Materials, 250014 Jinan, PR China

[2] Key Laboratory of Processing and Testing Technology of Glass & Functional Ceramics of Shandong Provincial, School of Materials Science and Engineering, Qilu University of Technology (Shandong Academy of Sciences), 250353 Jinan, PR China

**Highlights**

Particle morphology within $Al_2O_3$ aerogel changed due to the inhibited crystallization.

Fiber-like particles enhance strength but reduce specific surface area.

The optimized $Al_2O_3$ aerogel composites possessed a thermal conductivity of 0.136 W/m K at 1000 °C.

**Keywords** Alumina aerogel · Alumina-titania diphasic aerogel · Mechanical strength · Thermal stability · Thermal conductivity

## 1 Introduction

Aerogels, as a kind of nanoporous material with a high porosity of more than 90%, are synthesized by the sol–gel method and supercritical drying [1, 2]. Silica ($SiO_2$) aerogel and the derivatives [3–5] have a long history and are the most widely explored aerogels. However, these aerogels decompose and/or sinter at a relative high temperature [6]. Alumina ($Al_2O_3$) aerogel exhibits the enhanced thermal stability which is better than those of the other oxide aerogels, e.g., zirconia [7], titania ($TiO_2$) [8], and niobia [9]. In addition, $Al_2O_3$ aerogel exhibits ultralow thermal conductivity [10] and excellent catalytic activity [11]. Due to the fascinating properties, $Al_2O_3$ aerogel has great potential applications as high-temperature thermal insulator and catalyst [12]. Generally, the practical applications of aerogel have always been restricted due to their instinctive fragility and sintering behavior upon high temperature. Unfortunately, it is no exception to $Al_2O_3$ aerogel if it is used under loading and/or high temperature. Thermal conductivity of $Al_2O_3$ aerogel shows drastic increase after heat treatment above 800 °C (0.298 W/m K) [13]. Therefore, the mechanical strength and thermal stability of $Al_2O_3$ aerogel need to be further improved.

Kucheyev et al. [14] demonstrated that $Al_2O_3$ aerogel with excellent mechanical properties can be made by elaborately tuning the crystallographic phase, particle shape, and size of nanoligaments in the aerogel. Zu et al. [15, 16] casted $SiO_2$ thin film on the skeleton of $Al_2O_3$ aerogel via a post-gelation method to form an $Al_2O_3$ core-$SiO_2$ shell structure. The created core–shelled structure improves the mechanical properties of $Al_2O_3$ aerogel. The Young's modulus of the core–shelled $Al_2O_3$ aerogel is as high as 6.7 MPa, which is nearly four times higher than that of the pristine one. However, those methods are sophisticated and time consuming. It is worth noting that earlier studies have shown that mechanical strength and thermal stability can be improved by the addition of dopants. Hurwitz et al. [17] proposed $Al_2O_3$–$SiO_2$ diphasic aerogel. The obtained diphasic aerogel at an $Al_2O_3$:$SiO_2$ ratio of 3:1 retains mesoporous structure up to a very high temperature of 1200 °C. Benad et al. [18] created a robust $Al_2O_3$-based diphasic aerogel via combining the toughness of $Al_2O_3$ and the hardness of $ZrO_2$. With 20 mol% $ZrO_2$ dopants, Young's module of the diphasic aerogel reaches a maximum of 10.8 MPa.

$TiO_2$ is an efficient opacifier due to its high reflection index and strong broad-band adsorption [19–22]. It also can be used as dopants for modifying $Al_2O_3$ aerogel. Some works on $Al_2O_3$–$TiO_2$ diphasic system have reported. Hurwitz et al. [22] proposed the addition of $TiO_2$ influences the viscosity and gelation time of boehmite sol as well as the specific surface area (SSA), pore size distribution (PSD), and crystalline phase of $Al_2O_3$ aerogel. However, boehmite powders were adopted as $Al_2O_3$ source in their synthesis routes during which the homogeneous distribution of $TiO_2$ could not be realized. In order to obtain a more uniform doping, Wang et al. [23] prepared $Al_2O_3$–$TiO_2$ diphasic aerogel by using potassium titanate and tetrabutyl titanate as precursors. According to the study [24], high-concentrated (≥40 mol%) $TiO_2$ dopants within $Al_2O_3$ aerogel result in phase separation, during which $TiO_2$ grows into crystalline anatase particles. On the contrary, when the concentration of $TiO_2$ is low enough, $TiO_2$ is homogeneous dispersed in $Al_2O_3$ aerogel matrix. Erkalfa et al. [25] proposed that, when the concentration of $TiO_2$ in $Al_2O_3$ is less than 17.5 mol%, $TiO_2$ is substantially dissolved in $Al_2O_3$ aerogel. Although the synthesis of $Al_2O_3$–$TiO_2$ diphasic aerogels was well explored, their mechanical strengths and thermal properties upon high temperature were not fully studied. Since $Al_2O_3$–$TiO_2$ diphasic aerogels are brittle and shrunken when being subjected to loading and high temperature, the knowledges of their mechanical and thermal properties are still of interest for technical applications as well as theoretical researches.

Herein, in this work, we first synthesized a series of $Al_2O_3$ aerogels with and without minor $TiO_2$ dopants (up to 10 mol%) for realizing a homogeneous dispersion of $TiO_2$ in $Al_2O_3$ aerogels. Then, the mechanical strengths and pore structures of the synthesized aerogels and the aerogels heat-treated at 1000 °C were comprehensively studied. The changes of physical properties of the $Al_2O_3$ aerogels due to $TiO_2$ dopants were evaluated and the corresponding mechanism was proposed. At last, magnesium silicate ceramic fibers reinforced $Al_2O_3$ aerogel composites with the sizes of 20 cm width × 20 cm length × 1 cm thickness were fabricated for investigating thermal conductivity and possibility for the use as high-temperature thermal insulator.

## 2 Experimental section

### 2.1 Chemicals

All reagents were of analytical grade or higher and used as received without further purification. Aluminium chloride hexahydrate ($AlCl_3{\cdot}6H_2O$, Aladdin, AR, 97%), butyl titanate (TBOT, Kemiou, 98%), anhydrous ethanol (EtOH, Fuyu, 99.5%), Nitric acid (68%, Kangde), distilled water (DI water), propylene oxide (PO, aladdin, 99%), magnesium silicate ceramic fibers (Luyang Energy-Saving Materials Co., Ltd.).

### 2.2 Synthesis of $Al_2O_3$–$TiO_2$ diphasic aerogels

In a typical synthesis, 4.83 g $AlCl_3{\cdot}6H_2O$ was dissolved in 17.6 ml of a 50/50 v/v mixture of DI water and EtOH. In other bakers, 0.296, 0.430, and 0.882 ml TBOT was dissolved into a certain amount of EtOH at room temperature respectively. Nitric acid was added dropwise into the $TiO_2$ sol to reduce the hydrolysis and polycondensation rate. The molar ratio of TBOT:EtOH:nitric acid was set as 1:19.1:0.42. Finally, $Al_2O_3$ and $TiO_2$ sols were mixed to produce a bi-component sol in which the mole fractions of $TiO_2$ were 3, 5, and 10 mol%, respectively. Subsequently, 5.7 ml of PO was added into the sol under vigorous stirring for 10 min. The gelation occurred within about 25 min under room temperature. After gelation, the wet gels were demolded, aged, and solvent exchanged with EtOH for a few days. Then the wet gels were put into an autoclave containing certain amount of EtOH. After it was sealed, ultrapure, dry nitrogen gas was flushed in the autoclave to produce an oxygen free atmosphere and as a safety precaution. The autoclave temperature was raised to 270 °C while the pressure rose and was controlled at ~9 MPa for 2 h, and the autoclave was then decompressed slowly at a rate of 30 kPa/min. Finally, the system was cooled to room temperature naturally and the aerogels were removed. The pure $Al_2O_3$ aerogel and those with 3, 5, and 10 mol% $TiO_2$ dopants were denoted as A, A-3T, A-5T, and A-10T, respectively.

### 2.3 Synthesis of fiber reinforced aerogel composites

First, raw magnesium silicate ceramic fibers were cut into pieces with the sizes of 20 cm length × 20 cm width × 1 cm thickness. After being degassed in a self-made vacuum apparatus for 10 min, they were impregnated with A and A-10T sol, from which the samples were donated as A-fiber and A-10T-fiber, respectively. Ensuring no bubbles coming out from the composites any more, the composites within modules were proceeded to gelation under room temperature. The gelation times of the composites were a little longer than those of pure aerogels. After total gelation, the wet composited bodies were solvent exchanged, aged, and supercritical dried to obtain fiber reinforced aerogel composites.

### 2.4 Characterization

The XRD was performed on a Bruker D8 advance X-ray diffractometer at 40 kV and 100 mA with CuKα ($\lambda =$ 1.540598 Å) radiation, employing a scanning rate 5° per min in the 2θ ranging from 10° to 80°. The IR spectra were recorded on a Nicolet 5DX-FT-IR spectrometer using the KBr pellet method in the range of 4000–375 $cm^{-1}$. Supercritically dried aerogels were characterized by physical measurement to determine shrinkage and physical densities. Nitrogen gas adsorption–desorption at 77 K measured by JW-BK112 surface area and pore size analyzer after the samples were evacuated at 180 °C for 5 h under vacuum. The PSD and the pore volume (PV) were determined via the BJH (Barret–Joyner–Halenda) method from the adsorption curve. Transmission electron microscopy (TEM) images were recorded using a JEM-200CX electron microscope operating at 20 kV. Compressive strength of the aerogel was measured by using a WDW-5 Electronic Testing Machine under a quasi-static condition at a cross head speed of 1 mm/min. The thermal conductivities were measured by a high temperature thermal conductivity tester (DRS-III).

## 3 Results and discussion

The crystal phases of the as-dried aerogels were investigated first. Figure 1 provides the XRD patterns for pure $Al_2O_3$ aerogel and those with $TiO_2$ dopants. The pure $Al_2O_3$ aerogel showed crystalline boehmite phase with broad diffraction peaks, indicating small crystallite sizes of the boehmite. The diffraction peaks at 14.3°, 28°, 38.2°, 49.3°, 64.9°, and 71.8° were matched well with boehmite (JCPDS.21-1307). With $TiO_2$ dopants, no crystalline $TiO_2$ was found in all doped aerogels but the crystalline boehmite. With the increase of $TiO_2$ dopants, the diffraction peak at 14.8° and 71.8° disappeared. As the continuous increase of $TiO_2$, the diffraction peak at 38.2° gradually vanished, indicating that the crystallization of boehmite was inhibited. According to the study [26], in aqueous, $Al^{3+}$ ions exist as the unhydrolyzed species of $[Al(OH)_6]^{3+}$ below pH = 3; with increasing pH, $[Al(OH_2)_6]^{3+}$ hydrolyzes into $[Al(OH)_h(OH_2)_{6-h}]^{(3-h)+}$ ($h = 0$–4) which is the building block for crystalline boehmite. As shown in the following section, Fig. 3e exhibits the crystalline structure of boehmite; seen from the picture, crystalline boehmite consists of arranged $[AlO_6]$ octahedra which maybe derived from the hydrolysis and polycondensation of the $[Al(OH)_h$

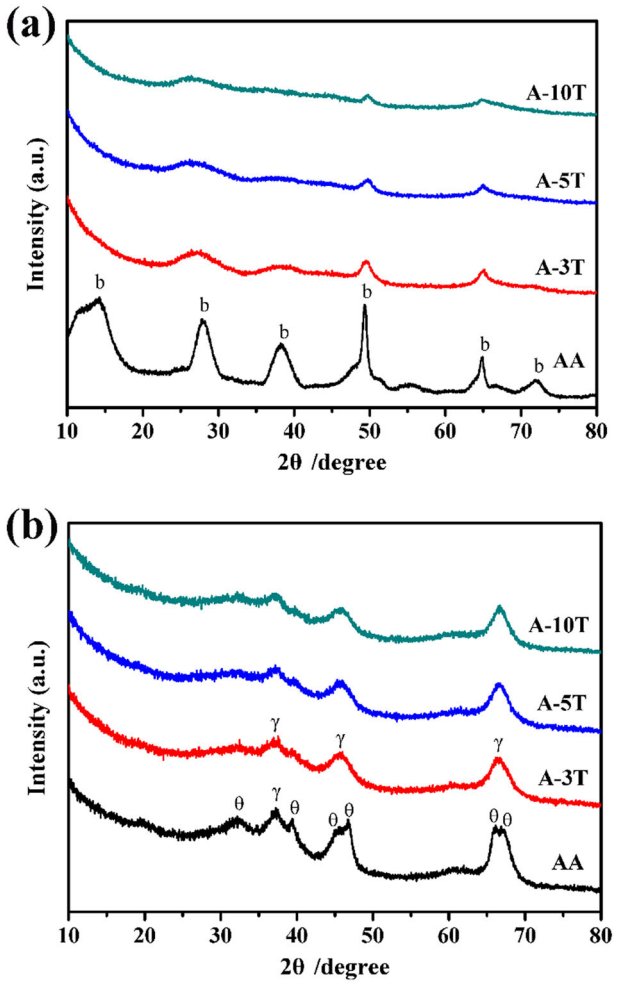


**Fig. 1** XRD patterns of pure $Al_2O_3$ aerogel and those with $TiO_2$ dopants (**a**) before and (**b**) after heat-treatment at 1000 °C for 2 h

$(OH_2)_{6-h}]^{(3-h)+}$. It is reasonable to presume that any factors affecting the hydrolysis and polycondensation of $[Al(OH)_h(OH_2)_{6-h}]^{(3-h)+}$ are capable to influence the crystallization of boehmite. During our experiment, we tested the initial pH value after mixing $Al_2O_3$–$TiO_2$ bi-component sol and they were 2.75, 2.49, 2.15, and 1.89 for A, A-3T, A-5T, and A-10T, respectively, mainly due to the acidities of $TiO_2$ sol (i.e., both the nitric acid and TBOT are acidic in $TiO_2$ sol). The added PO gel initiator increased the pH value of the bi-component sol, as a consequence, both $[Al(OH)_h(OH_2)_{6-h}]^{(3-h)+}$ and TBOT were proceeded to hydrolysis and condensation. As we measured the decreased pH value upon the addition of $TiO_2$ sol, it could be deduced that, the hydrolysis and polycondensation of $[Al(OH)_h(OH_2)_{6-h}]^{(3-h)+}$ were retarded to some extent, resulting in the inhibited crystallization of boehmite. On the other hand, according to the sol–gel chemistry of transition metal oxides [27], the introduced nitrate ions within $TiO_2$ sol would serve as complexed ligands toward $[Al(OH)_h(OH_2)_{6-h}]^{(3-h)+}$, decreasing the reactivity of hydrolysis and condensation. Herein, it would expect that the introduced nitrite ion is another factor accounting for the inhibited crystallization of boehmite. After heat treatment at 1000 °C for 2 h, as shown in the diffraction patterns (Fig. 1b), phase transition occurred in the pure $Al_2O_3$ aerogel. The $Al_2O_3$ aerogel changed from boehmite to γ-$Al_2O_3$/θ-$Al_2O_3$. As consequences of $TiO_2$ doping, γ-$Al_2O_3$ was observed as the main phase in the doped $Al_2O_3$ aerogels, indicating that $TiO_2$ hinders the phase transition of the $Al_2O_3$ aerogel to a certain extent. Although the heat-treatment was implemented at a high temperature of 1000 °C and a long duration of 2 h, the crystalline $TiO_2$ was not observed in the doped $Al_2O_3$ aerogels that supports the fact that there is no segregation or agglomeration of the secondary phase of $TiO_2$ if the doped concentration is low. As a result, the homogeneous and advantageous structure developed during sol–gel process was preserved. γ-$Al_2O_3$ has a cation-deficient spinel structure and can easily react with metal oxides [28]. Therefore, we suggested that $TiO_2$ dopants may stabilize the oxygen lattice and there with retard the phase transition of γ-$Al_2O_3$ to θ-$Al_2O_3$. A similar conclusion has also been reported by Smith et al. [29] and Sun et al. [30].

Figure 2 shows the FT-IR spectra of pure $Al_2O_3$ aerogel and those with $TiO_2$ dopants before and after heat-treatment. As shown in Fig. 2a, the bands at 3423 and 1630 $cm^{-1}$ are ascribed to –OH stretching and H–O–H bending vibration, respectively [31], indicating the presence of surface hydroxyls and absorbed water molecules. For the pure $Al_2O_3$ aerogel, the bands at 1068, 735, 616, and 473 $cm^{-1}$ are the characteristic adsorption bands of boehmite due to $[AlO_6]$ octahedrons [15]. The small band near 870 $cm^{-1}$ indicates the presence of some $[AlO_4]$ species [32]. Upon the doping of $TiO_2$, the above-mentioned adsorption peaks, which are ascribed to $[AlO_6]$ octahedrons and $[AlO_4]$ tetrahedrons, were also detected and contributed by boehmite. However, the peak intensities weakened obviously, indicating the inhibited crystallization due to the $TiO_2$ dopants. In addition, the decreased intensity of the peak at 3090 $cm^{-1}$, which had been assigned to the –OH stretching of AlOOH [22], further proves the incorporation of $TiO_2$ deteriorating the crystallinity of boehmite. As shown in Fig. 2b, after heat-treatment at 1000 °C, the characteristic peaks of boehmite disappeared. A broad band at 500–1000 $cm^{-1}$ appeared and could be assigned to the characteristic $[AlO_4]$ tetrahedrons in γ-$Al_2O_3$ [32]. The absorption bands at 547 and 612 $cm^{-1}$ are attributed to the O–Al–O bending and A–O stretching vibrations of $[AlO_6]$ octahedrons. The peaks demonstrate the phase transition from boehmite to γ-$Al_2O_3$ which is basically consistent with those results of XRD.

TEM was used to understand the microstructures of pure $Al_2O_3$ aerogels and $TiO_2$-doped $Al_2O_3$ aerogels. As shown in Fig. 3a, the pure $Al_2O_3$ aerogel consisted of fiber-like particles with the diameters of 2–5 nm and the lengths of 30–80 nm. The fiber-like particles were interconnected into

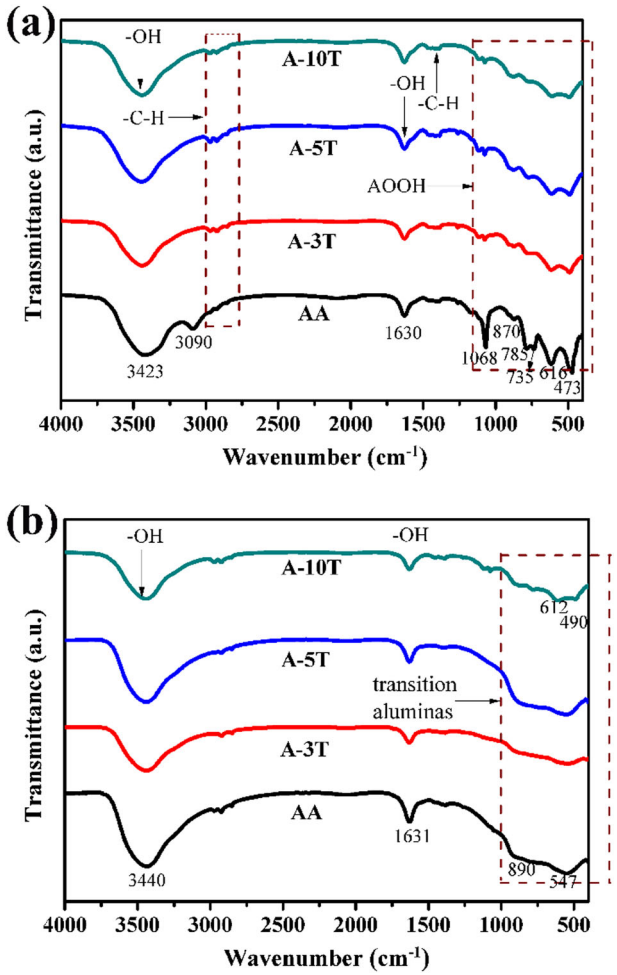


**Fig. 2** FT-IR spectra of pure $Al_2O_3$ aerogel and those with $TiO_2$ dopants (**a**) before and (**b**) after heat-treatment at 1000 °C for 2 h

a complicated network. During the formation of boehmite fibers, some polymeric clusters (<1 nm), which contained [$AlO_6$] octahedra, would form first via the hydrolysis and polycondensation of the mentioned $[Al(OH)_h(OH_2)_{6-h}]^{(3-h)+}$. These clusters are likely to continue to grow via various growth mechanisms, e.g., Ostwald ripening and Oriented attachment. As shown in Fig. 3e, the crystal structure of boehmite consists of [$AlO_6$] octahedra arranged in parallel layers linked by the hydrogen bonds of interstitial water molecules a long [010] direction. Due to the weak hydrogen bonds, thermodynamically, it is easy for the polymeric clusters to continue to grow along [010] direction via the formation of hydrogen bonds, resulting a preferential growth and one-dimensional boehmite with fiber-like morphology. Based on theoretical calculations, Mercuri et al. [33] also demonstrated that one dimensional boehmite along [010] direction is more preferential than the others of growth directions due to the high surface energy of (010) facets. Herein, the fiber-like particles are possibly because of the preferential and directional crystal growth of boehmite. However, significant variations on particle morphologies were observed upon the doping of $TiO_2$. As shown in Fig. 3b, with the increase of $TiO_2$ dopant, unlike the pure $Al_2O_3$ aerogel that is composed of fiber-like particles, the A-3T changed into very fine fibrous and spherical particles. With the further increase of $TiO_2$ dopants, the fiber-like particles gradually decreased and replaced by some spherical particles. With 10 mol% $TiO_2$ dopants, the fiber-like particles were rarely observed in the TEM image (Fig. 3d). The skeleton of A-10T was comprised of loose connected spherical particles as shown in Fig. 3d. Herein, it could be concluded that the incorporation of $TiO_2$ significantly changes the morphologies of the particles within $Al_2O_3$

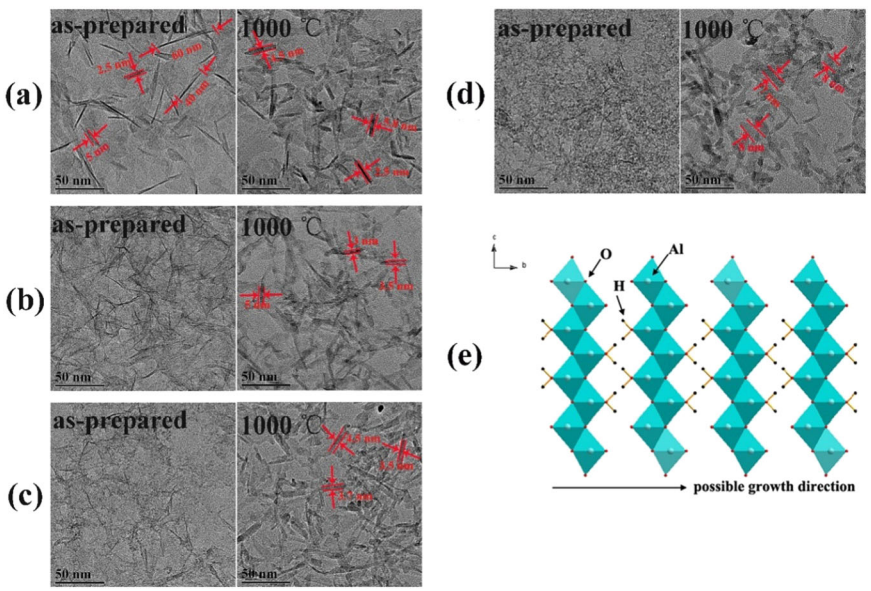


**Fig. 3** TEM images of **a** pure $Al_2O_3$ aerogel, **b** A-3T, **c** A-5T, and **d** A-10T aerogels before and after heat-treatment at 1000 °C for 2 h. **e** crystal in structure of boehmite

aerogel. The morphology evolutions shown in TEM are correlative with the XRD and IR results in which show that $TiO_2$ dopants inhibit the crystallization of boehmite. Based on the correlation, it can ascribe the transition from fiber-like morphology to sphere-like morphology to the inhibited crystallization of boehmite. The morphologies transitions of $Al_2O_3$ aerogels due to metal cation dopants have been found in other works, e.g., shuttle-like particles in $Fe^{3+}$-doped $Al_2O_3$ aerogel [34], honeycomb mesh structure in $Ni^{2+}$-doped $Al_2O_3$ aerogel [35]. The morphologies of the pure $Al_2O_3$ aerogel and those with $TiO_2$ dopants heat-treated at 1000 °C for 2 h were also studied via TEM. The pure $Al_2O_3$ aerogel retained the fiber-like particles with the thicknesses of 2–6 nm, larger than that of the non-heat-treatment. For the aerogel with $TiO_2$ dopants, the sphere-like particles all turned into fiber-like particles, maybe due to the enhanced crystallization which had been proved by XRD measurements. As for A-3T and A-5T, the aerogels showed fiber-like particles with the thicknesses of 1–5 nm. They were 3–8 nm for the A-10T, larger than that of the pure $Al_2O_3$ aerogel.

The microstructural differences resulted in varying mechanical properties. The mechanical properties of $Al_2O_3$ aerogels were determined via uniaxial compress test. Before the test, the densities were calculated from the measured weight divided by the volume. Due to the inherent fragility, the failures of $Al_2O_3$ aerogels showed a certain randomness. For reliable compress test results, each compressive strength was determined by six samples. The stress–strain curves (Fig. S1) are typical brittle material characters that the stresses were suddenly dropped down when loads exceeded specific values. The values were identified as the compressive strengths. The results of mechanical strengths are shown in Fig. 4. As shown in Fig. 4a, the densities of pure $Al_2O_3$ aerogel, A-3T, A-5T, and A-10T aerogels were $0.109 \pm 0.001$ g/cm$^3$, $0.127 \pm 0.002$ g/cm$^3$, $0.138 \pm 0.001$ g/cm$^3$, and $0.151 \pm 0.002$ g/cm$^3$, respectively. Although, the densities increased with the increase of $TiO_2$ dopants, pure $Al_2O_3$ aerogel was more robust (0.23 MPa) than those with $TiO_2$ dopants (0.02–0.17 MPa). The Young's moduli decreased with the increase of $TiO_2$ dopants, showing the same trend as to the compressive strength. Yoldas et al. [36] pointed out that the mechanical behavior depends on the connectivity of secondary particle. Poco et al. [37] proposed that the high crystallinity and the highly connected fiber-like particles of boehmite maybe responsible for the enhanced mechanical properties. In terms of our compressive strength results, it also can be concluded that $Al_2O_3$ aerogel with the fiber-like particles (i.e., pure $Al_2O_3$ aerogel) is significantly stiffer and more robust than those with the sphere-like particles (i.e., those with $TiO_2$ dopants). When being under loading, the $Al_2O_3$ aerogel with fiber-like particles was pressed tightly and the fibers interweaved with each other to

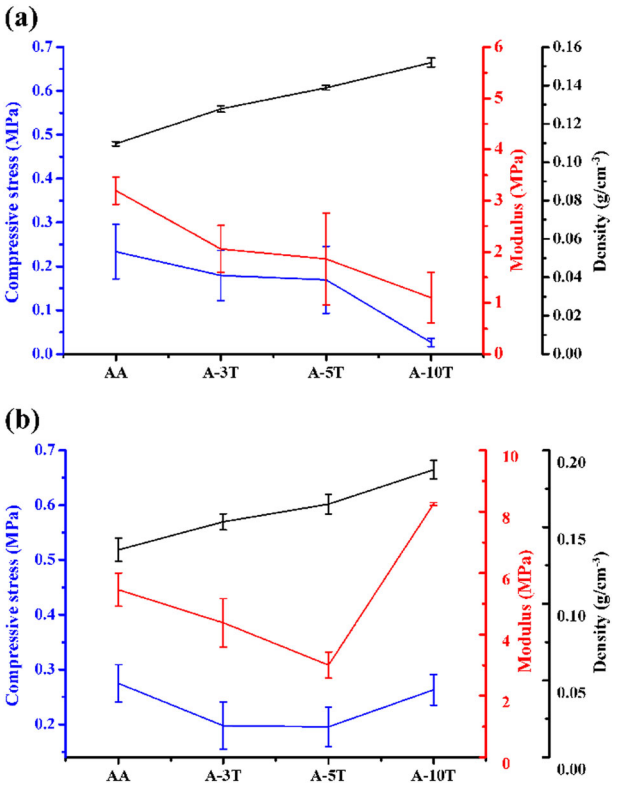


**Fig. 4** Densities, compressive stresses, and modulus of the dried aerogels (**a**) and the aerogels after being heat-treated at 1000 °C (**b**)

strengthen mechanical properties. Therefore, the better mechanical strength of our pure $Al_2O_3$ aerogel compared to those with $TiO_2$ dopants is maybe due to the interconnected fiber-like particles. Diphasic aerogels, e.g., $Al_2O_3$–C [38] and $Al_2O_3$–$SiO_2$ [39], were claimed that have enhanced mechanical strengths compared to that of the individual $Al_2O_3$ aerogel. With $Al_2O_3$–C diphasic aerogel as example, it exhibited a fiber-like particles/sphere-like particles hybrid network. The interactions between boehmite nanofibers were enhanced via the incorporated sphere-like particles. Herein, these diphasic aerogels performed enhanced mechanical strengths. For our studies, with increasing $TiO_2$ dopants, the boehmite fiber-like particles themselves turned into spherical particles rather than the fiber-like particles/sphere-like particles hybrid network. We think the decreased mechanical properties as the doping of $TiO_2$ is reasonable.

For further exploring the origin of mechanical robustness of $Al_2O_3$ aerogel, these aerogels were heat-treated at 1000 °C for 2 h. The mechanical strengths were studied. Figure 4b collects the evolutions of densities, compressive stresses, and moduli of the aerogel after heat-treatment. The densities of pure $Al_2O_3$ aerogel, A-3T, A-5T, and A-10T aerogels were $0.135 \pm 0.007$, $0.153 \pm 0.005$, $0.164 \pm 0.006$, and $0.187 \pm 0.005$ g/cm$^3$, respectively, larger than those without heat-treatment, indicating the densifying of aerogels

during heat-treatment. Correspondingly, the mechanical strengths were overall enhanced. The compressive strength of pure $Al_2O_3$ aerogel was 0.27 ± 0.03 MPa, slightly larger than that without heat-treatment. The strengths of A-3T and A-5T aerogels showed a decrease compared to that of pure $Al_2O_3$ aerogel. However, the strength of A-10T aerogel was 0.26 ± 0.02 MPa, presenting a bounce as compared to those of A-3T and A-5T aerogel. Even, its Young's modulus dramatically increased to 8.3 MPa, much larger than other $Al_2O_3$ aerogel, indicating the highest stiffness among the $Al_2O_3$ aerogels. Combining the TEM results, the increase of mechanical strength of A-10T compared to those of A-3T and A-5T comes from two following reasons: (1) the sphere-like particles turned into the fiber-like particles; (2) the connections between particles were enhanced as shown in the TEM results. The findings further prove the fiber-like particles enhance the strength of $Al_2O_3$ aerogel.

Figure 5a shows $N_2$ adsorption/desorption isotherms and PSDs of $Al_2O_3$ aerogels before heat-treatment. The $Al_2O_3$ aerogels exhibited type IV isotherm curves with type H1 hysteresis loop. At a relative low pressure of 0–0.8, the gradual rises of adsorption volume result from multilayer adsorption on the external surface of pores. The abrupt increase stages and the hysteresis loops between 0.8 and 1.0 are attributed to the capillary condensation of $N_2$ molecules in mesopores with the diameters of 2–50 nm. When relative pressure closed to 1, the adsorption was still unsaturated, indicating macropores with the diameters larger than 50 nm. Although the isotherms (Fig. 5a) demonstrated the characters of meso- and macro-pores within the pure $Al_2O_3$ and A-3T aerogels; however, as shown in Fig. 4c, the PSD curves showed nonobvious peak during the range of mesopores. With the further increase of $TiO_2$ dopants, the $Al_2O_3$ aerogel performed typical mesoporous characters with some adsorption peaks located in the range of 20–60 nm. This is due to the fiber-like particles gradually turned into sphere-like particles. The fluffy accumulation between fiber-like particles is easy to form macropores; the compact packing of sphere-like particles is more likely to form micro- and meso-pores in terms of geometry. The SSA, PV, and pore diameter are listed in Table 1, the SSA of $Al_2O_3$ aerogels with $TiO_2$ dopants improved significantly as compared to that of pure $Al_2O_3$ aerogel. The SSA of A-3T was 650 $m^2/g$, nearly two times larger than that of the pure $Al_2O_3$ aerogel (326 $m^2/g$). The PVs of $Al_2O_3$ aerogels with $TiO_2$ dopants were larger than that of the pure $Al_2O_3$ aerogel. The sphere-like particles morphology may contribute to the high SSAs and high PVs of $Al_2O_3$ aerogels with $TiO_2$ dopants. Even after heat-treatment at 1000 °C, the $Al_2O_3$ aerogels with $TiO_2$ dopants performed higher PVs and higher SSAs than those of pure $Al_2O_3$ aerogel as shown in Table 1.

$Al_2O_3$ aerogel and its derivatives are considered as the potential candidates of high temperature thermal insulating materials. In purpose of determining thermal conductivities, we built composite structures which consist of $Al_2O_3$

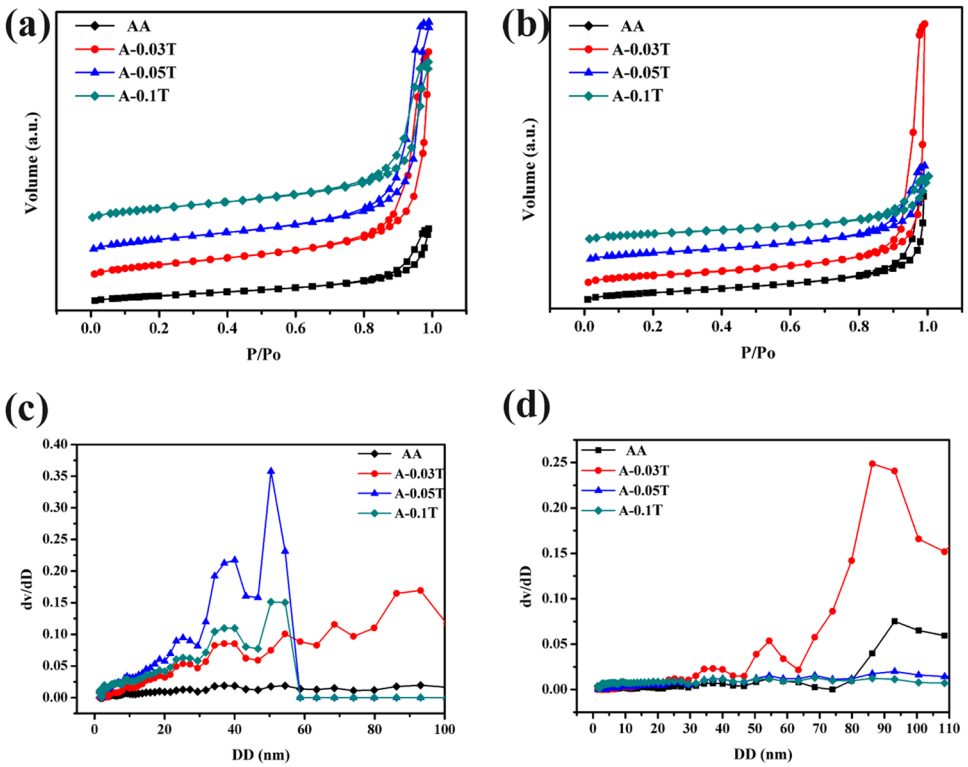


**Fig. 5** $N_2$ adsorption/desorption isotherms of pure $Al_2O_3$ aerogel and those with $TiO_2$ dopants (**a**) before and (**b**) after heat-treatment at 1000 °C for 2 h, **c**, **d** are their corresponding pore diameter distributions, respectively

**Table 1** Textural properties of the $TiO_2$-doped $Al_2O_3$ aerogels after drying and after heat-treatment at 1000 °C

| | SSA ($m^2$/g) | | PV ($cm^3$/g) | | PD (nm) | |
|---|---|---|---|---|---|---|
| | As-prepared | 1000 °C | As-prepared | 1000 °C | As-prepared | 1000 °C |
| $Al_2O_3$ | 326 | 277 | 1.0 | 0.9 | 9.8 | 11.8 |
| A-3T | 650 | 302 | 3.3 | 2.2 | 15.1 | 25.7 |
| A-5T | 648 | 296 | 3.4 | 0.8 | 15.3 | 10.1 |
| A-10T | 630 | 224 | 2.3 | 0.5 | 11.5 | 8.4 |

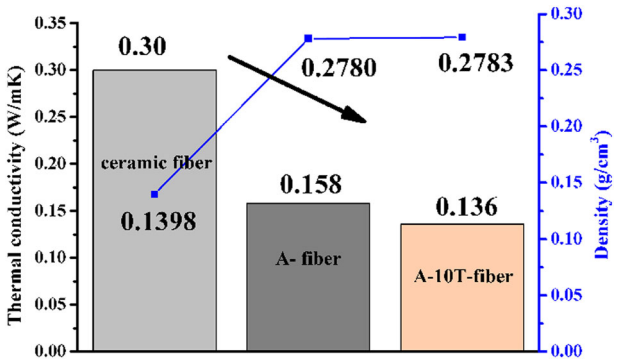


**Fig. 6** Thermal conductivities of ceramic fiber blanket, $Al_2O_3$ aerogel composite with and without $TiO_2$ dopants

aerogels and magnesium silicate ceramic fibers. After sol–gel and supercritical drying process, $Al_2O_3$ aerogel composites were achieved. Such composite configuration improved both the ease of handling and the overall thermal resistance of aerogels. As shown in Fig. 6, the densities of fiber blanket, $Al_2O_3$ aerogel composites and $Al_2O_3$ aerogel composites with $TiO_2$ dopants were 0.139, 0.278, and 0.279 g/$cm^3$, respectively; the thermal conductivity of the fiber reinforced $Al_2O_3$ aerogel composite at 1000 °C was 0.158 W/m K, which was much lower than that of the ceramic fiber blanket (0.30 W/m K). Although the density of the aerogel composite was larger than that of the ceramic fiber blanket, the thermal insulating performance of the aerogel composite seems to be much better than that of the ceramic fiber blanket. This is because the impregnation of $Al_2O_3$ aerogel greatly restricts the convection heat transfer of gas within the composite [16]. The influence of skeleton heat transfer of $Al_2O_3$ aerogel within the composite could be almost omitted. Moreover, we found that doping of $TiO_2$ could further improve thermal insulating performance, endowing the composites a lowest thermal conductivity of 0.136 W/m K at 1000 °C. The low thermal conductivity of the fiber reinforced $Al_2O_3$ aerogel composite with $TiO_2$ dopants at 1000 °C is lower than the pure $Al_2O_3$ aerogel (0.298 W/m K at 800 °C [13]) as well as other thermal insulation materials such as $Al_2O_3$ aerogel/mullite fiber composite (0.16 W/m K) [16], commercial polycrystalline mullite fiber (0.30 W/m K) [40], indicating its potential application as high-temperature thermal insulator.

## 4 Conclusions

In summary, we synthesized and studied a series of $Al_2O_3$ aerogels with and without $TiO_2$ dopants. The main conclusions are as follow:

(1) The pure $Al_2O_3$ aerogel, which had the fiber-like particles, was stronger than those with $TiO_2$ dopants that presented the sphere-like particles. The sphere-like particles turned into fiber-like particles after heat-treatment accompanied with the enhanced mechanical strengths of the $TiO_2$-doped $Al_2O_3$ aerogel.
(2) The sphere-like particles of $TiO_2$-doped $Al_2O_3$ aerogel contributed the largest SSA (648 $m^2$/g), much larger than that of the pure $Al_2O_3$ aerogel (326 $m^2$/g). Herein, it can be concluded that the fiber-like particles enhance strength but reduce SSA.
(3) The thermal conductivity of ceramic fibers reinforced $Al_2O_3$ aerogel composite with 10 mol% $TiO_2$ dopants possessed a thermal conductivity of 0.136 W/m K at 1000 °C, indicating the potential application as high-temperature thermal insulator.

**Acknowledgements** This work was supported by the National Natural Science Foundations of China (No. 21603125), Shandong Provincial Natural Science Foundation of China (ZR2017BEM009), Youth Science Funds of Shandong Academy of Sciences (2018QN0031), Youth Science Funds of Qilu University of Technology (Shandong Academy of Sciences) (2018QNHZ02), and Science and Technology projects of Shandong Province (ZR2018LE003) are acknowledged for financial support.

## Compliance with ethical standards

**Conflict of interest** The authors declare that they have no conflict of interest.

## References


1. Hüsing N, Schubert U (2010) Aerogels-airy materials: chemistry, structure, and properties. Angew Chem Int Ed 37:22–45
2. Dorcheh AS, Abbasi MH (2008) Silica aerogel; synthesis, properties and characterization. J Mater Process Tech. 199:10–26
3. Zu G, Shimizu T, Kanamori K, Zhu Y, Maeno A, Kaji H, Shen J, Nakanishi K (2018) Transparent, superflexible doubly cross-linked polyvinylpolymethylsiloxane aerogel superinsulators via ambient pressure drying. ACS Nano 12:521–532
4. Zu G, Kanamori K, Maeno A, Kaji H, Nakanishi K (2018) Superflexible multifunctional polyvinylpolydimethylsiloxane-based aerogels as efficient absorbents, thermal superinsulators, and strain sensors. Angew Chem Int Ed 57:9722–9727
5. Zu G, Kanamori K, Shimizu T, Zhu Y, Maeno A, Kaji H, Nakanishi K, Shen J (2018) Versatile double-cross-linking approach to transparent, machinable, supercompressible, highly bendable aerogel thermal superinsulators. Chem Mater 30:2759–2770
6. Emmerling A, Gross J, Gerlach R, Goswin R, Reichenauer G (1990) Isothermal sintering $SiO_2$-aerogels. J Non-Cryst Solids 125:230–243
7. Dong JS, Park TJ (1996) Sol–gel strategies for pore size control of high-surface-area transition-metal oxide aerogels. Chem Mater 8:509–513
8. Suh DJ, Park TJ, Han HY, Lim JC (2002) Synthesis of high-surface-area zirconia aerogels with a well-developed mesoporous texture using $CO_2$ supercritical drying. Chem Mater 141:452–1454
9. Campbell LK, Na BK, Ko EI (1992) Synthesis and characterization of titania aerogels. Chem Mater 4:1329–1333
10. Keysar S, Shter GE, Hazan YD, Cohen AY, Grader GS (1997) Heat treatment of alumina aerogels. Chem Mater 9:2464–2467
11. Hirashima H, Kojima C, Imai H (1997) Application of alumina aerogels as catalysts. J Sol–Gel Sci Technol 8:843–846
12. Pierre AC, Pajonk GM (2002) Chemistry of aerogels and their applications. Chem Rev 102:4243–4265
13. Xu L, Jiang Y, Feng J, Feng J, Yue C (2015) Infrared-opacified $Al_2O_3$-$SiO_2$ aerogel composites reinforced by SiC-coated mullite fibers for thermal insulations. Ceram Int 41:437–442
14. Kucheyev SO, Baumann TF, Cox CA, Wang YM (2006) Nanoengineering mechanically robust aerogels via control of foam morphology. Appl Phys Lett 89:041911
15. Zu G, Shen J, Zou L, Wang W, Lian Y, Zhang Z, Du A (2013) Nanoengineering super heat-resistant, strong alumina aerogels. Chem Mater 25:4757–4764
16. Zu G, Shen J, Wang W, Zou L, Lian Y, Zhang Z, Liu B, Zhang F (2014) Robust, highly thermally stable, core-shell nanostructured metal oxide aerogels as high-temperature thermal superinsulators, adsorbents, and catalysts. Chem Mater 26:5761–5772
17. Hurwitz FI, Gallagher MT, Olin C, Shave MK, Ittes M, Olafson KN, Fields MG, Rogers RB (2014) Optimization of alumina and aluminosilicate aerogel structure for high-temperature performance. Int J Appl Glass Sci 5:276–286
18. Benad A, Jurries F, Vetter B, Klemmed B, Hubner R (2018) Mechanical properties of metal oxide aerogels. Chem Mater 30:145–152
19. Kwon YG, Choi SY, Kang ES, Baek SS (2000) Ambient-dried silica aerogel doped with $TiO_2$ powder for thermal insulation. J Mater Sci 35:6075–6079
20. Kuhn J, Gleissner T, Schuster MCA, Korder S, Fricke J (1995) Integration of mineral powders into $SiO_2$ aerogels. J Non-Cryst Solids 186:291–295
21. Wang J, Kuhn J, Lu X (1995) Monolithic silica aerogel insulation doped with $TiO_2$ powder and ceramic fibers. J Non-Cryst Solids 186:296–300
22. Zhang H, Qiao Y, Zhang X, Fang S (2010) Structural and thermal study of highly porous nanocomposite $SiO_2$-based aerogels. J Non-Cryst Solids 356:879–883
23. Yang J, Wang Q, Wang T (2017) Effects of Ti addition on alumina/titania composite aerogels synthesized by Sol–Gel process and supercritical ethanol drying. J Chin Chem Soc 64:978–985
24. Hurwitz FI, Rogers RB, Sheets EJ, Miller DR, Newlin KN (2012) Influence of Ti addition on boehmite-derived aluminum silicate aerogels: structure and properties. J Sol–Gel Sci Technol 64:367–374
25. Erkalfa H, Misirli Z, Baykara T (1998) The effect of $TiO_2$ and $MnO_2$ on the densification and microstructural development of alumina. Ceram Int 24:81–90
26. Baes CF, Mesmer RE (1976) The hydrolysis of cations. Wiley, New York
27. Livage J, Henry M, Sanchez C (1988) Sol–gel chemistry of transition metal oxides. Prog Solid State Chem 18:259–341
28. Bolt PH, Habraken FHPM, Geus JW (1998) Formation of nickel, cobalt, copper, and iron aluminates from α- and γ-alumina-supported oxides: a comparative study. J Solid State Chem 135:59–69
29. Smith JS (2012) The synthesis and structural characterization of metal oxide nanoparticles having catalytic applications. https://scholarsarchive.byu.edu/etd/3667. Accessed 3 July 2012
30. Sun X, Wu Y, Wang Y, Li M (2019) Investigation of the effect of lanthanum oxide on the thermal stability of alumina aerogel. J Porous Mater 26:327–333
31. Wu L, Huang Y, Wang Z, Liu L, Xu H (2010) Fabrication of hydrophobic alumina aerogel monoliths by surface modification and ambient pressure drying. Appl Surf Sci 256:5973–5977
32. Hurwitz FI, Rogers RB, Guo H, Yu K, Domanowski J, Schmid E, Fields MG (2017) The role of phase changes in maintaining pore structure on thermal exposure of aluminosilicate aerogels. MRS Commun 7:1–9
33. Mercuri F, Costa D, Marcus P (2009) Theoretical investigations of the relaxation and reconstruction of the γ-AlO(OH) boehmite (101) surface and boehmite nanorods. J Phys Chem C 113:5228–5237
34. Ren L, Li X, Cui S (2016) Synthesis of monolithic $Fe_2O_3$–$Al_2O_3$ composite aerogels via organic solvent sublimation drying. J Nanomater 2016:8135043
35. Li X, He H, Cui S, Ren L (2012) Synthesis and characterization of the monolithic NiO-$Al_2O_3$ aerogels. Am J Anal Chem 3:946–949
36. Yoldas BE (1992) In: Hench L, West JKChemical Processing of Advanced Materials. Wiley, New York
37. Poco JF, Satcher JH, Hrubesh LW (2001) Synthesis of high porosity, monolithic alumina aerogels. J Non-Cryst Solids 285:57–63
38. Zhong Y, Kong Y, Shen X, Cui S, Yi X, Zhang J (2013) Synthesis of a novel porous material comprising carbon/alumina composite aerogels monoliths with high compressive strength. Microporous Mesoporous Mater 172:182–189
39. Hayase G, Nonomura K, Kanamori K, Maeno A, Kaji H, Nakanishi K (2016) Boehmite nanofiber-polymethylsilsesquioxane core-shell porous monoliths for a thermal insulator under low vacuum conditions. Chem Mater 28:3237–3240
40. Saran G (2012) Investigation of refractory thermal insulation material. https://ieeexplore.ieee.org/abstract/document/6357515. Accessed 18–21 Sept 2012